
This is an electronic reprint of the original article.
This reprint may differ from the original in pagination and typographic detail.

Ajdary, Rubina; Kretzschmar, Niklas; Bani Asadi, Hossein; Trifol Guzman, Jon; Seppälä, Jukka; Partanen, Jouni; Rojas Gaona, Orlando

Selective Laser Sintering of Lignin-Based Composites

Published in:
ACS Sustainable Chemistry and Engineering

DOI:
[10.1021/acssuschemeng.0c07996](https://doi.org/10.1021/acssuschemeng.0c07996)

Published: 22/02/2021

Document Version
Peer-reviewed accepted author manuscript, also known as Final accepted manuscript or Post-print

Please cite the original version:
Ajdary, R., Kretzschmar, N., Bani Asadi, H., Trifol Guzman, J., Seppälä, J., Partanen, J., & Rojas Gaona, O. (2021). Selective Laser Sintering of Lignin-Based Composites. *ACS Sustainable Chemistry and Engineering*, 9(7), 2727-2735. <https://doi.org/10.1021/acssuschemeng.0c07996>

This material is protected by copyright and other intellectual property rights, and duplication or sale of all or part of any of the repository collections is not permitted, except that material may be duplicated by you for your research use or educational purposes in electronic or print form. You must obtain permission for any other use. Electronic or print copies may not be offered, whether for sale or otherwise to anyone who is not an authorised user.

Selective Laser Sintering of Lignin-based Composites

Rubina Ajdary,¹ Niklas Kretschmar,² Hossein Baniasadi,³ Jon Trifol,³ Jukka V. Seppälä,³

Jouni Partanen,² Orlando J. Rojas^{1,4}*

¹Department of Bioproducts and Biosystems, School of Chemical Engineering, Aalto University, P.O. Box 16300, FIN-00076 Aalto, Espoo, Finland.

²Department of Mechanical Engineering, School of Engineering, Aalto University. P.O. Box 12150, FIN-00076 Aalto, Espoo, Finland.

³Department of Chemical and Metallurgical Engineering, School of Chemical Engineering, Aalto University, P.O. Box 16300, FIN-00076 Aalto, Espoo, Finland.

⁴Bioproducts Institute, Departments of Chemical and Biological Engineering, Chemistry and Wood Science, University of British Columbia, 2360 East Mall, Vancouver, BC Canada V6T 1Z3.

* Corresponding Author: orlando.rojas@aalto.fi, [+358505124227](tel:+358505124227)

Abstract

Lignin is introduced as a suitable component for selective laser sintering (SLS) of polyamide (PA12) to reduce costs while maintaining or improving processability and performance. Alkali lignin (sourced as a polydisperse, amorphous powder) was used at a volume concentration of up to 60 vol% for 3D-printing complex, layered structures. The latter were obtained as high axial aspect objects, produced in the flat, flipped (90°), and vertical directions, which were further examined to elucidate the effect of lignin as a suitable component in SLS. The

composite withstood heating during SLS and sintered PA/lignin showed 30% less degradation at elevated temperature compared to pure PA. The morphological, wetting, mechanical, and thermal characteristics associated with the 3D-printed structures were compared. For instance, the strength and wettability were highly dependent on processing orientation. Compared to objects produced from neat PA, those that included lignin presented a higher porosity (~10%) with a simultaneous increase in stiffness (increased Young modulus, by ~16%, and reduced tensile strength, by ~7%). Owing to differences in surface roughness and composition, an important difference in the water contact angle (CA) of the samples printed in the flipped and flat orientations were observed (55° and 126°, respectively). Overall, SLS is shown as a developmental step toward lignin valorization in composites while allowing reduced cost, scalability, and facile processing.

Keywords: Lignin, polyamide, selective laser sintering, additive manufacturing

Introduction

Lignin is one of the main biopolymers in plants and accounts for about 30% of non-fossil organic carbon in the biosphere.¹ Although lignin is abundantly available, it has a complex and chemically diverse structure, with relatively low reactivity and processability, depending on the source. So far, lignin utilization has been mostly limited to energy generation in boilers while the balance, a minor portion, is used for animal feed, as a natural binder, adhesive, and in coatings, among others.²⁻⁶

Along with delignifying wood in typical pulping processes, considerable amounts of technical lignins can be made available for high-value chemicals from biomass as well as low-cost by-products.^{7,8} Technical lignins can offer promise when applied as fillers in polymer composites, e.g., for use as a stabilizer and antioxidant and compounding with polyolefins.⁹⁻¹¹ Recently, several studies have focused on lignin as a reinforcing filler and as an alternative to carbon

black in rubber manufacturing, for example, toward the production of green tires. However, fundamentally, mixing quality and interfacial interactions remain the most important challenges that need to be addressed.^{12,13}

Composite films have been reported with 5% to 15% biorefinery/organosolv lignin in polylactic acid (PLA). The thermal stability and brittleness of the composites were enhanced compared to pure PLA, whereas the tensile strength decreased.¹⁴ Such latter effect is mostly associated with the inhomogeneous dispersion of lignin particles and the interfacial incompatibility with the polymer matrix.¹⁵⁻¹⁷ The challenges to uniformly disperse lignin can be addressed by its (surface) modification or improving the mixing efficiency. Lignin-containing composites can be processed with conventional manufacturing techniques such as injection molding as well as layer-by-layer additive manufacturing (AM). Lignin as a filler or reinforcing agent has been successfully tested at loadings of up to 15% in several AM processes, including fused deposition molding (FDM)¹⁸ and resin-based stereolithography (SLA).¹⁹ In this context, lignin has been typically employed as a substitute for conventional polymer matrices to reduce material cost and enhance the share of the bio-based composition. The fabrication of parts solely consisting of lignin remains problematic due to its complex thermal behavior and brittleness. However, commercially available injection molding materials such as “arboform”,²⁰ which contain high levels of cellulose (~60 %), lignin (~30 %), and other natural additives, the latter used as a plasticizer, may represent valuable bio-based alternatives to those from fossil carbon.

Amongst a large number of available AM processes, selective laser sintering (SLS) represents one of the most relevant processes toward end-use components.^{21,22} Shortly, SLS uses a polymer powder that is spread as a bed, and a selected area is irradiated with a laser. The heated material sinters (SLS) or melts (selected laser melting, SLM), forming a solid layer. Hypothetically, all powders that tend to fuse under the exposure of a laser beam and solidify

rapidly, under adjustable processing conditions, are suitable for SLS. The classes of materials that fulfill these requirements include metals, ceramics, and some polymer.²³ Unfortunately, the materials typically used in SLS manufacturing are relatively more expensive given the required control on particle size, morphology, and size distribution. Therefore, there is a need for cost-effective alternatives while maintaining print quality. Importantly, aging of the powder under processing temperatures and storage time are two additional challenges in SLS, which also affect the mechanical and visual properties of the final product.^{24,25}

SLS can yield objects with complex geometries and high fidelity; alongside, SLS enables a comparatively high production rate and affords a wide selection of materials. To boost productivity, the SLS components can be fabricated with layer thicknesses of 60-180 μm , and up to four lasers can be used simultaneously. In such a process, the powder bed is preheated close to the sintering temperature to avoid significant temperature gradients, and the additional heating provided by the scanning laser(s) fuse the particles with the given spatial resolution.

Today, PA12 is the most frequently processed material in SLS and have, in fact, acquired industrial relevance.²⁶ This is due to its strength, dimensional flexibility, and heat resistance. PA12 has a balanced property profile suitable for SLS processing into structures with a wide range of applications.²² To address the environmental concerns related to materials derived from fossil-carbon, fully bio-based polymers, such as PA11 derived from castor oil, have been considered. However, the use of PA11 for SLS requires an inert gas chamber for processing.²⁷ In this study, a lignin/PA12 composite material is demonstrated as a way to valorize lignin and to produce low-cost, thermally stable, and strong SLS composites. To the best of our knowledge, this is the first report on the synthesis of highly loaded lignin SLS structures.

Materials

Alkali lignin powder was purchased from Sigma-Aldrich (47 - 51 % carbon content and sulfur < 3.6 %, particle size ranging from few microns to 40 μm). PA12 powder (Sinterit PA12 smooth, particle size of 18-90 μm) was obtained from Sinterit (Poland). Ethanol (ETAX Aa 99.5%, Finland) and distilled water were also utilized.

Methods and Characterization

Printing process. Initially, a certain amount of PA12 and alkali lignin dry powders were measured and mixed mechanically for several minutes using a rotating blender to obtain the desired volume/mass ratio. Afterward, the blended dry powder (lignin: PA 40:60 wt%) was immediately fed to the SLS system for pre-heating until reaching a temperature of 175 °C, which took approximately 50 min. Subsequently, sample fabrication started automatically. All samples were printed using an entry-level SLS called Sinterit Lisa with a maximum build volume of 150 mm \times 200 mm \times 150 mm, and an IR laser diode of 5 W. Instead of applying a deflection mirror system, we used a print head equipped with the laser scanning the cross-sectional areas of the sliced component. For mechanical testing, dog-bone shape samples (**Figure 1**) were printed with different orientations, including horizontal or flat (parallel to the platform), horizontally flipped by 90°, and vertical (perpendicular to the platform). The print was performed using a laser type IR diode (5 W, wavelength of 808 nm), for a print surface temperature of 174.5 °C and layer thickness of 0.125 mm. The conditions were determined from preliminary experiments to optimize the quality of printed samples. Throughout this discussion, the samples are referred to as *flat* (horizontally flat, parallel to the platform), *90°* (horizontal, flipped by 90°), and *vertical*, according to the printing orientation. The latter was shown to produce low print quality and was deemed not relevant for further comparison (see

Supporting Information). All printed samples were cold-dried at room temperature after SLS processing.

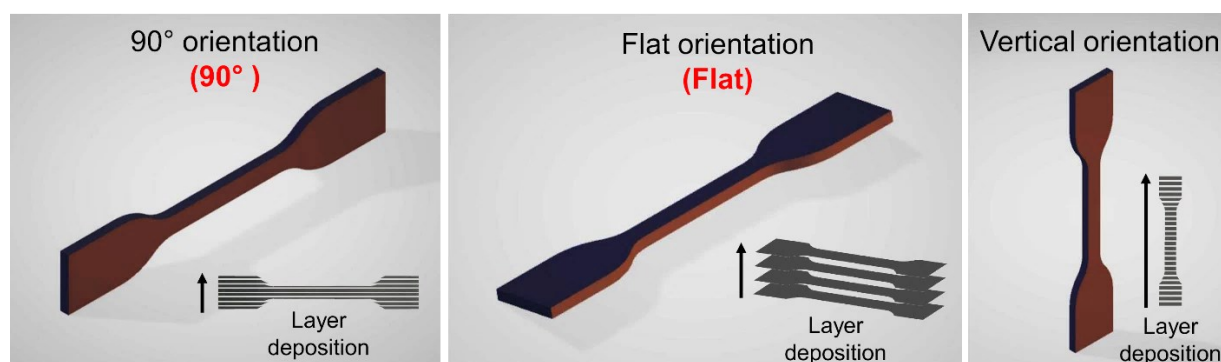


Figure 1. Dog bone objects 3D-printed using different layer deposition directions concerning the platform, from left to right: 90°, flat, and vertical.

The presence of lignin increased the overall temperature of the build envelope, which eventually caused a selective fusion of unscanned areas (**Figure S1**). This issue was even more noticeable in larger builds, for instance, during the printing of the vertical samples. Therefore, we applied a temperature offset of -3 °C compared to the default value (Note: the maximum possible temperature offset of -5 °C did not prevent the powder from fusing in the areas relevant to the actual component prevented printing of specimens in the vertical orientation). Preliminary tests using different lignin loadings were conducted, but the present discussion focused on the samples with a lignin content of 60 vol% (40 wt%), which was the maximum volume tested.

Differential scanning calorimetry (DSC). About 5 mg of sample was placed into a Tzero aluminum pan and sealed with a standard lid. The measurements were performed with a DSC (TA Instruments, MT-DSC Q2000, USA) using a scan rate of 5°C/min. Two heating/cooling cycles were employed. The melting enthalpy (ΔH_m) as well as the melting (T_m) and crystallization (T_c) temperatures were determined from the second cycle.

Thermogravimetric analysis (TGA). The thermal stability and the compositional degradation behavior of lignin, PA12, and their blends, before and after sintering, were studied by thermogravimetric analysis (TGA, TA Instruments Q500, USA) operated from 30 °C to 600 °C with a heating rate of 5 °C/min and under nitrogen atmosphere.

Microstructure. The microstructure of the powder and the laser-sintered sample was observed with a scanning electron microscope (SEM, Zeiss Sigma VP, Germany) operated at an accelerated voltage of 2 kV. Samples were fixed on metal stubs using double-sided carbon tape and sputtered with a layer of a thickness of 4 nm of gold-palladium alloy using a LEICA EM ACE600 (Leica, Germany) sputter coater before imaging.

Porosity. The porosity of the laser-sintered samples was evaluated by applying the ethanol replacement method.²⁸ Briefly, a sintered sample (6 mm × 6mm × 3 mm) was immersed in extra-pure ethanol, and the weight changes were monitored until reaching a constant value. The porosity Φ was calculated following **Equation 1**, where m_{sat} is the weight of the saturated sample, m_d (g) is the weight of the dried sample, ρ is the density of ethanol, and V is the apparent volume. The reported Φ values represent the average of three replicates.

$$\Phi (\%) = \left(\frac{m_{\text{sat}} - m_d}{\rho} \right) \times 100 \quad (1)$$

Density. The density ($\frac{\text{g}}{\text{cm}^3}$) of the SLS structures of defined geometry was simply calculated by dividing the weight of the sintered sample by its volume.

Surface area and pore volume. The surface area and pore volume were measured by N₂ adsorption on the solid at given relative pressures (Micromeritics Tristar II), following the Brunauer Emmett Teller (BET) and Barrett Joyner Halenda (BJH) models. Before the measurements, the samples were oven-dried at 120 °C overnight, and the degassing step was performed for 90 minutes at 120 °C.

Mechanical strength. Tensile testing was conducted following ASTM D638 Type IV (Instron 5944 system). The measurements were conducted at 23 °C and 50% RH with a load cell and a crosshead rate of 2 kN and 1 mm/min, respectively. The reported values are the average of 4-5 tested samples.

Water Contact angle. The wettability of the samples was measured by assessing the water contact angle (CA) of printed samples (90° and flat orientations) using a Theta Flex Optical Tensiometer. The contact angle of the water droplets was calculated from image analysis using the OneAttension software.

Fourier transform infrared spectrometry (FTIR). The chemical features of PA12 and lignin powders, as well as the blend and sintered sample, were evaluated using FTIR with ATR (PerkinElmer spectrum 100 FT-IR) operated at wavenumbers from 4000 to 500 cm^{-1} (resolution of 4 cm^{-1} , and rate of 32 scans).

Results and discussion

Thermal properties. For SLS, the powder needs to reach the sintering temperature (T_g), below the melting temperature (T_m), so that particles fuse to each other but avoiding undesired polymer melting, fusion, or degradation (**Figure S1**). To better understand thermal behavior at high temperatures and establish suitable printing conditions, the thermal behavior of the lignin, PA, and the mixture (60 vol% lignin, 40 vol% PA), before and after sintering, was studied by DSC and TGA. As an amorphous polymer, lignin undergoes physical changes under heating, transitioning into glassy and rubbery states at the T_g . According to the literature, the T_g of lignin is difficult to discern accurately, and a single value of T_g does not exist but rather a range (typically between 90 °C to 180 °C), depending on moisture content and lignin type.^{29,30} The

T_g of PA, with a relatively high degree of crystallinity, was assumed to be ~ 50 °C, according to reports from the literature.³¹

Compared to pure PA, the lignin/PA sample showed a fairly similar melting temperature; however, the crystallization temperature decreased slightly (**Figure 2a**, **Table 1**, and **Table S1** for mixed powder before sintering).³² The melting temperature of the samples (177 °C) was slightly higher than the print surface temperature (175 °C), which was a requirement for successful processing, e.g., to avoid unwanted fusion. The additional energy needed to sinter selective areas was provided by the laser; notably, temperature gradients between the print surface and melting points are ideally low to limit the risk of bending or twisting the structure. The degradation temperature of PA, lignin, and PA/lignin are shown in **Figure 2b**. As noted, the lignin had a slight mass loss (2 %) below 100 °C, which was attributed to the moisture; no substantial mass loss up to the printing temperature (177 °C) was recorded, which suggested that lignin could withstand the applied heating, without substantial degradation. Besides, the sintered PA/lignin showed no thermal degradation near the printing temperature region. Over 97% of pure PA was decomposed at elevated temperatures; however, compared to pure PA, the mass loss (77%) decreased in the lignin/PA composite. The DTG of pure lignin, DSC, and TGA analyses of mixed, non-sintered lignin/PA powders are shown in **Figure S2**, **Figure S3** and **Figure S4** respectively.

Table 1. The latent heat of melting (ΔH_m), melting (T_m), and crystallization (T_c) temperatures.

	ΔH_m (J/g)	T_m (°C)	T_c (°C)
PA	41.7	176.5	154.2
Lignin/PA, sintered	27.8	176.6	149

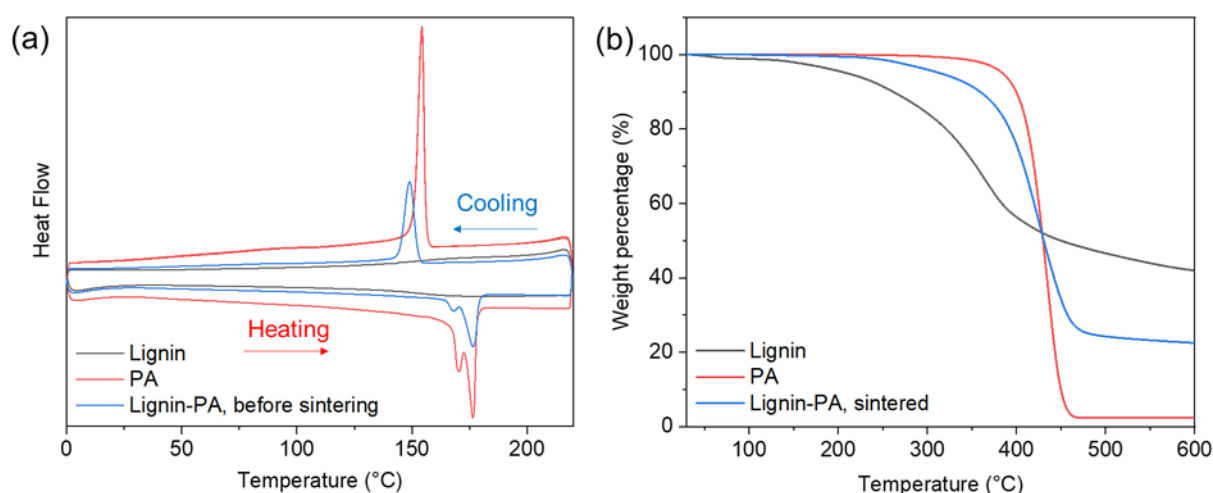


Figure 2. DSC scans of lignin, PA, lignin/PA (60:40 vol%) after sintering obtained during (a) heating and cooling cycle from 0 °C to 220 °C. (b) Thermogravimetric analysis of the samples tested from room temperature to 600 °C.

Microstructure. According to the SEM imaging, lignin powder particle sizes span the range from few microns to 40 μm (**Figure 3a**), making lignin a suitable filling material since smaller particles can fit void spaces, optimizing the packing. Compared to lignin, PA particles, **Figure 3b**, were larger (18-90 μm) and more homogeneous in size. The surface of pure SLS dog bones prepared with neat PA was rather uneven (*flat* and 90° orientation, **Figure 3c-d**). With the addition of lignin, the print quality was enhanced and resulted in smoother surfaces. The *flat* dog bone presented in **Figure 3f** shows even surfaces, considering that the surface comprises a single layer (as displayed in the layer depositions in **Figure 1**); however, the surface of the 90° sample included as many layers as the whole structure (**Figure 3e**). The polydispersity of lignin contributed to a relatively homogeneous surface structure in 90° and *flat* sintered samples, as indicated in **Figure 3e-f** (500X magnification). During material processing, PA particles melted under laser irradiation and fused with each other while entrapping the lignin component.

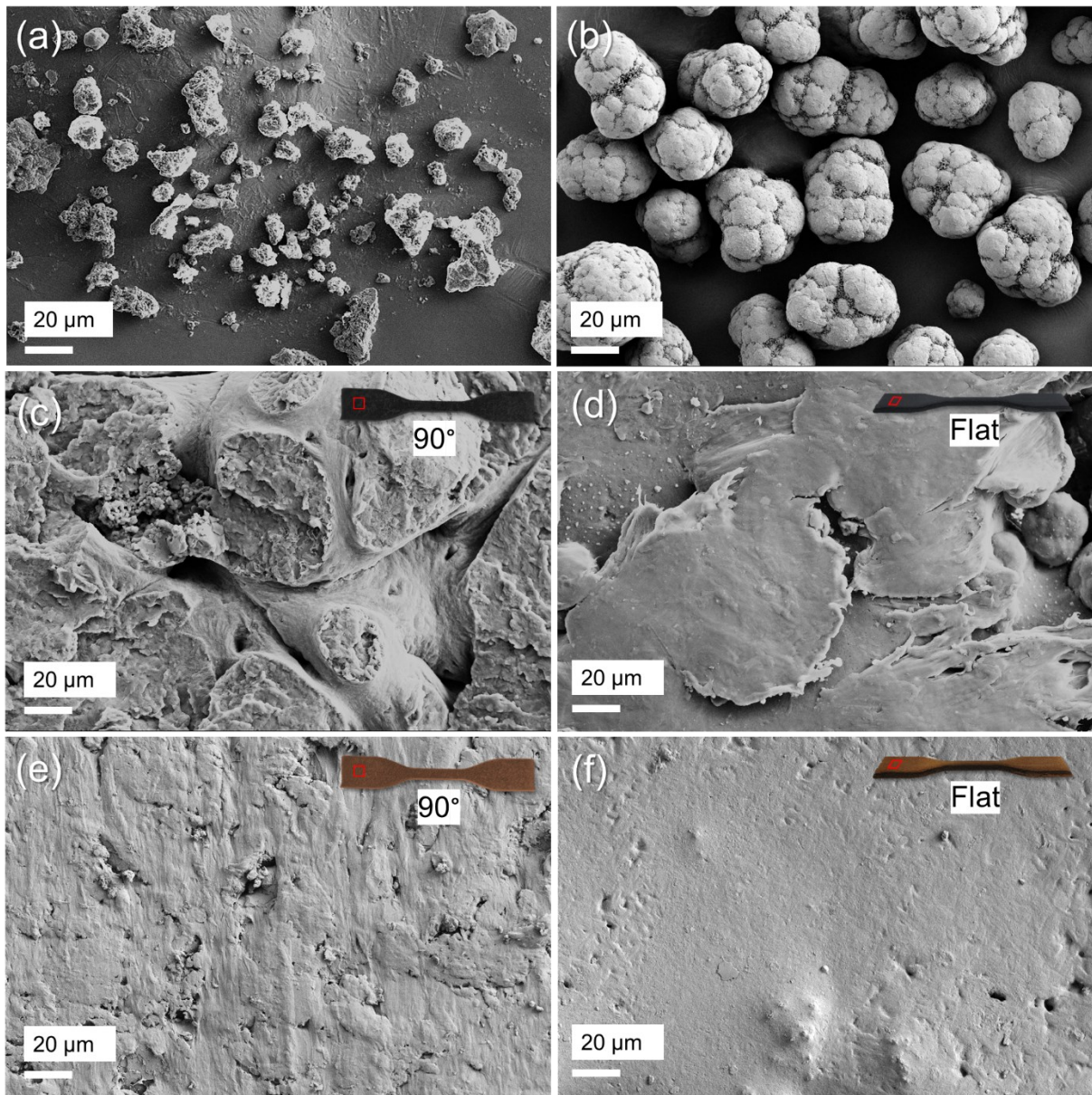


Figure 3. Scanning electron microscopy images of (a) lignin and (b) PA powders. Image of sintered neat PA (c) 90° and (d) *flat* samples. Also, the images of samples of sintered Lignin/PA composites are included: (e) 90°, and (f) *flat* samples. The lignin:PA volume ratio used was 60:40 vol%. All images correspond to 500X magnification.

The layer thickness in print settings was adjusted to 0.125 mm, according to the standard mode used for neat PA, as defined by the manufacturer (Sinterit's standard mode). In addition to laser power, other variables contribute to a high degree of powder sintering, including the laser spot size, scan speed, size and dispersity of the sintering particles.³³ On one hand, low laser power,

high layer thickness, and fast scanning speed may provide a limited energy density to sinter the polymer and merge the layers effectively. On the other hand, high laser power, low layer thickness, and low scan speed can result in substantial material evaporation.³⁴ Therefore, a proper balance of processing parameters is required to achieve a high print quality and to fulfill the mechanical performance requirements of the developed structure. The cross-section of layers printed from neat PA was relatively packed, and most of the PA particles were fused, as shown in **Figure 4a-b**. With the addition of lignin, the laser beam fused the polyamide on the surface ($\sim 40 \mu\text{m}$ on the top part of the layer thickness) and prevented the laser beam from reaching the bottom section of each layer, thus limiting PA fusion (**Figure 4c**). However, the SEM image of the non-fused area obtained at larger magnifications, **Figure 4d**, shows a combination of fused and non-fused PA in the presence of lignin.

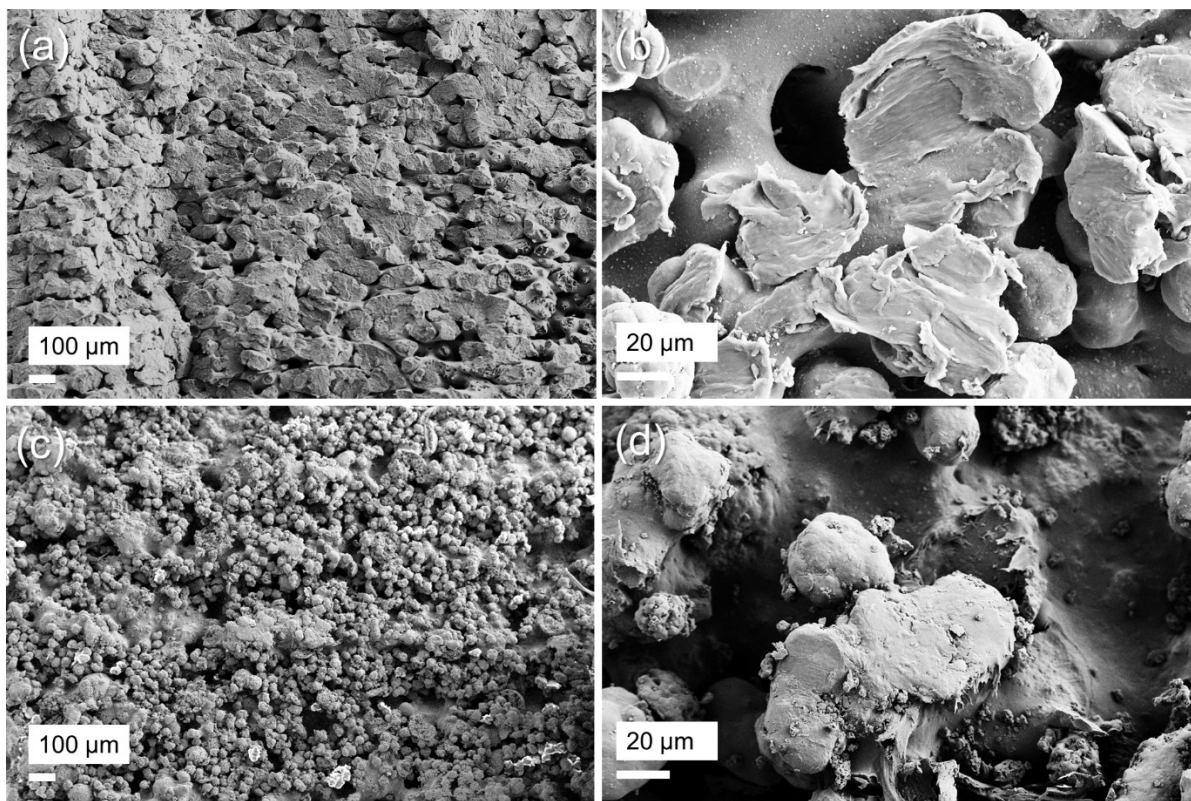


Figure 4. SEM cross-section images of samples printed by SLS: neat PA at (a) 50X and (b) 500X magnifications, lignin/PA composite at (c) 50X and (d) 500X magnifications.

Surface area, porosity, and density. The porosity of the sintered samples, which is summarized in Table 2, was similar in both 90° and flat printing directions, 12 and 14%, respectively. The porosity was substantially higher than that of pure sintered PA12, 4%. The increased porosity in lignin/PA composites was likely due to the incomplete fusion of some PA particles and the dispersion of lignin powder that randomly packed the particles during the deposition of layers in SLS. As Table 2 indicates, after the laser sintering and fusion, the samples presented a surface area of 2.15 m².g⁻¹ (90° orientation) and 0.94 m².g⁻¹ (flat orientation). The low values of total pore volume in **Table 2** indicated a limited availability of micropores (< 2 nm) and mesopores (2-50 nm) in the microstructure. The N₂ adsorption-desorption isotherms for sintered lignin/PA fit the type IV adsorption isotherm and the H3 hysteresis loop typical of narrow slit pores presented in regions of micropores; no plateau was observed at high P/P⁰ (**Figure S5**). Finally, the density of the composites (90° and flat orientations) were higher than pure PA, by ~20% and 30%, respectively; which was expected since the lignin powder (1.3 g.cm⁻³) had a higher density at room temperature compared to PA (1.01 g.cm⁻³). However, the layer by layer deposition and random packing of particle mixture during the SLS process resulted in obtaining structures with slightly higher porosity than pure PA.

Table 2. The BET surface area, porosity, and density of lignin/PA sintered samples in the 90° and flat orientations.

Sample	BET surface area, m ² .g ⁻¹	External surface area, m ² .g ⁻¹	Average pore diameter, nm	Total volume in pores, cm ³ .g ⁻¹	Porosity (ethanol replacement), %	Density, g. cm ⁻³
90°	2.15	1.93	4.4	0.00224	12	1.2 ± 0.07
Flat	0.94	0.91	5.5	0.00120	14	1.3 ± 0.06

Mechanical properties. As shown in **Figure 5**, the lignin/PA sample (90°) showed better mechanical properties (modulus strength and strain at break) than that produced with the flat orientation. As discussed earlier in the microstructure section, the more extensive fusing of PA

layers in the 90° orientation resulted in enhanced modulus and ultimate strength compared with the flat sample, comprising a lower number of layers. The incorporation of 60 vol% lignin in the 90° orientation sample substantially increased the Young Modulus, by 16%, along with a small reduction (7%) in the stress at break. This latter reduction might be attributed to the higher porosity of the composite (14%) compared to the neat PA (4%).

Compared with neat PA processed *via* injection molding (IM) and FDM, the samples produced by SLS showed a lower strength (**Figure 5c**), which could be due to heat-driven processing efficiency achieved by injection molding and FDM, enabling fusion of the PA powder. In addition, the polymer chain alignment following the FDM technique is known to be an effective factor in enhancing the mechanical strength. A similar trend in strength reduction has been reported for PA reinforced with metal particles and graphene, using low power lasers (< 6 W).³⁵ Moreover, for neat PA, an increased laser power to 10 W improved the fusion and resulted in higher tensile strength compared to the sample sintered at lower laser power.³⁶

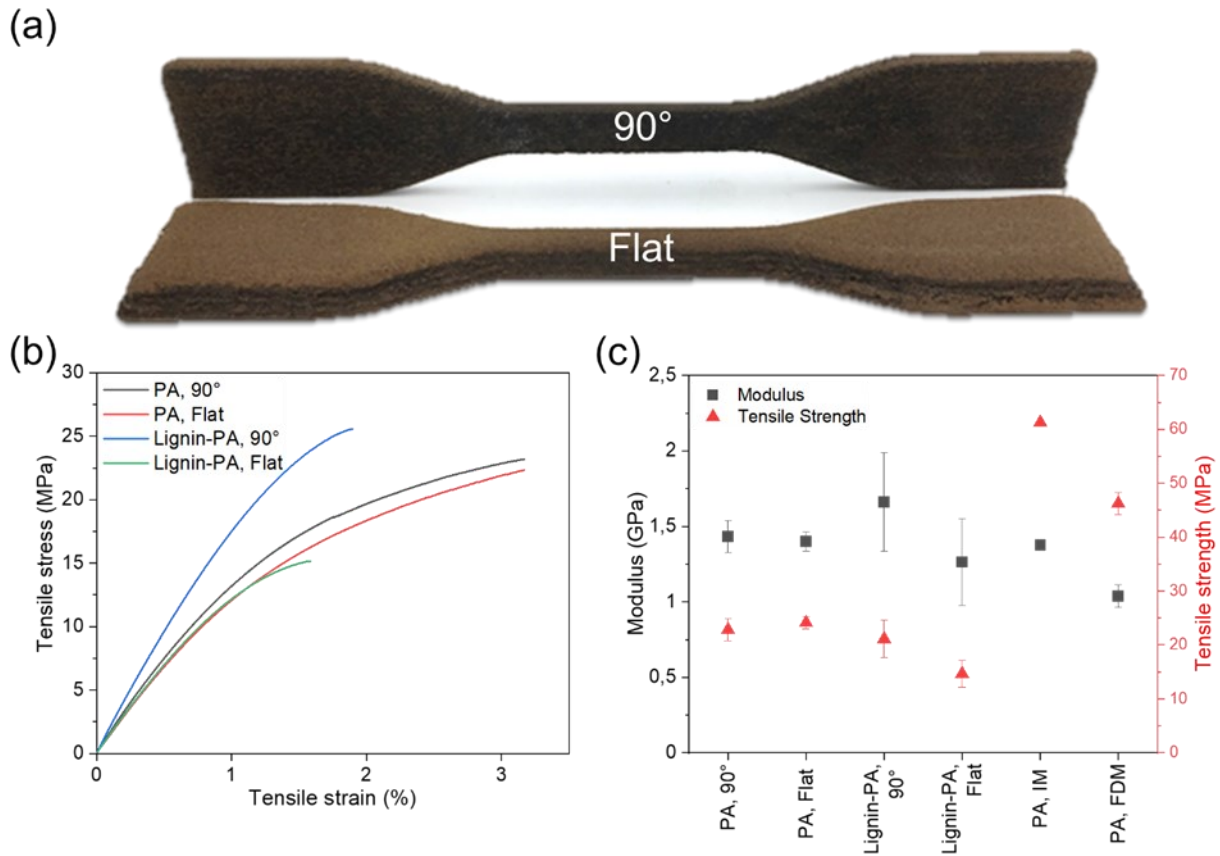


Figure 5. Samples fabricated using the 90° and flat orientations and results of mechanical strength (ASTM D638 Type IV tensile testing): (a) lignin/PA sintered composites (lignin: PA 40:60 wt%), (b) tensile strain-stress behavior, and (c) comparison of elastic modulus and ultimate tensile strength of lignin/PA in 90° and flat orientations with samples obtained from neat PA using SLS, FDM, and IM.

Wettability. According to the contact angle measurements, the lignin/PA composite processed in flat orientation presented a higher water contact angle (CA=126°) compared to the sample printed at 90° orientation (CA=55°) (**Figure 6a-b**). Given the effect of roughness on CA, the results are likely due to the higher surface roughness of the latter sample (**Figure 3e-f**). The pure PA sample presented a contact angle of 91° in the 90° print orientation and 113° in the flat one. Compared to the flat print orientation, the 90° print orientation introduced a higher surface roughness since it included several horizontal layers (the surface of the flat sample was formed by a single layer). Furthermore, lignin was likely to be more concentrated on the surface of the

sample with flat orientation (it visually appeared to be more brownish), which might point to the possibility of material/chemical partitioning, an issue that remains for further studies.

Chemical characterization. The samples were analyzed by FTIR spectrometry to rationalize the major difference in the contact angles of 90° and samples with flat orientation (**Figure 6c**). The PA and composite samples showed a peak at 3293 cm⁻¹, associated with hydrogen-bonded N-H stretching.³⁷ In addition, the intensity of a moderate peak corresponding to the amide bond at 3098 cm⁻¹ reduced from neat PA to 90° orientation composite (a minimum intensity was observed in the sample printed in a flat orientation). The C-N stretching vibration and CO-NH bending appeared at 1538 cm⁻¹ and 1539 cm⁻¹ in the neat PA and composites, with a clear reduction in the intensity of the peaks.^{38,39} A peak at 1512 cm⁻¹ in lignin spectra corresponding to the aromatic ring^{40,41} was also shown, albeit with less intensity in lignin-containing composites. Furthermore, the sample printed with a 90° orientation showed a change at 1734 cm⁻¹ compared to pure PA, attributed to C=O vibration on *p*-coumaroyl groups in lignin.⁴² The lower peak intensities observed for the sample printed in a flat direction compared to those of neat PA and 90° orientation may relate to the contribution of surface chemical composition on the surface wetting, as previously assessed by the water contact angle values.

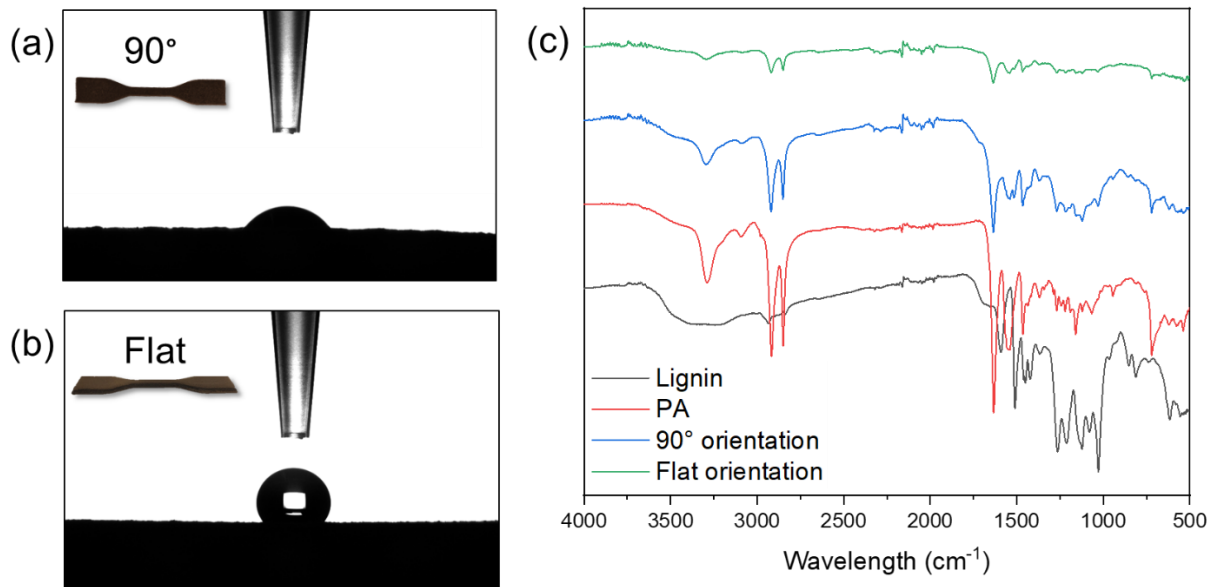


Figure 6. Images of a water droplet used to measure the contact angle of samples processed in (a) 90° and (b) flat orientation. (c) Chemical characterization (FTIR-ATR spectra) of sintered samples for lignin, PA, and the sintered samples at 90° and flat orientation.

Processing of complex structures. Ultimately, the SLS of lignin/PA opens the possibility of manufacturing complex geometries (such as gradient surface-based lattice structures), possibly with high fidelity and resolution. As such, an object with a complex geometry was printed by a scalable SLS process (**Figure 7**). The results indicated the possibility of lignin/PA as an alternative polymer system for the fabrication of cost-effective, additively manufactured components. While our experiments were carried out with composites with a lignin content of 60 vol%, higher loadings may still be feasible. To enable enhanced process control, a study on the powder/laser interaction of such powder blends is necessary, *e.g.*, to avoid printing defects and to guarantee enhanced sintering behavior. In this context, surface-modified lignin might allow higher levels of adhesion with the PA particles. As far as economics, while industrial lignin powders are rather inexpensive, the manufacturing cost of spherical lignin particles (micro and nano-sized beads produced by aerosol flow systems) is estimated to be between 0.9 and 1.2 USD/kg,^{43,44} which may constitute an ideal component, given their morphology. On

the other hand, the cost of PA12 is much higher compared to lignins, about 50-60 USD/kg.⁴⁵ Hence, there is a large potential for lignin utilization in additive manufacturing, e.g., to develop low-cost, thermally stable, biobased composites. In fact, fully biobased composites are expected if PA12 is replaced with bio-based polyamides, such as PA11 from castor oil.

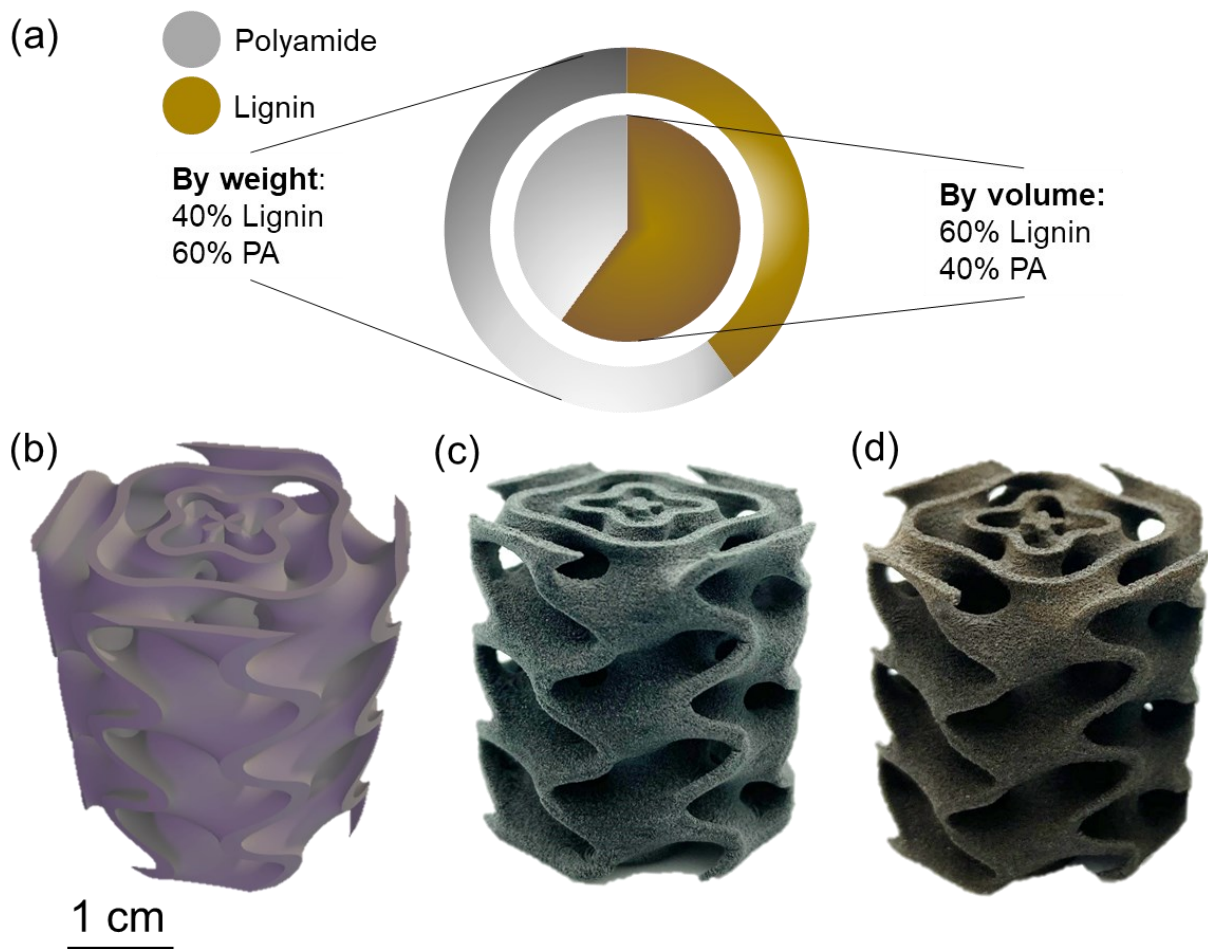


Figure 7. (a) Lignin loading in our experiments (volume- and weight % of lignin in PA powder) for the fabrication of samples via SLS. (a) A surface-lattice structure used as a demonstration for added design complexity in SLS. (b) 3D model of the lattice structure fabricated by SLS with (c) neat PA and (d) lignin/PA (lignin: PA 60:40 vol%).

Keeping in mind that no report is available on the 3D printing of lignin/PA composites, we compared the mechanical properties of our samples with those of other lignin-based 3D printed composites reported in the literature (**Table 3**). Few reports discuss lignin/PA composites prepared by traditional melt blending methods. The tensile modulus and strength of the

lignin/PA12 samples were better or in good agreement with those of the literature. The results support the potential of the SLS technique for preparing high lignin-content lignin/PA composite, as a route toward low-cost, bio-based systems for engineering applications.

Table 3. Comparison of lignin-based composites with varying lignin content and manufacturing processes (additive and conventional methods).

Material	Lignin content, wt%	Process	Strength, MPa	Young's modulus, GPa	Ref.
Lignin- PA, 90°	40.00	SLS	21	1.7	This work
Lignin- PA, flat	40.00	SLS	14.6	1.3	This work
Lignin- PLA	20.00	FDM	18	-	46
Lignin- PLA	40.00	FDM	27	1.7	47
Lignin- poly(L-lactic acid)	40.00	Compressed molded	23.2	1.2	48
Lignin- Methacrylate resin	0.40	SLA	49	2.25	49
Lignin- Polyurethane acrylate/morpholine/tri propylene glycol diacrylate	3.00	SLA	8	0.004	50
Lignin- Ethoxylated pentaerythritol tetraacrylate/aliphatic urethane acrylate/urethane acrylate	15	SLA	15	0.37	19

Conclusions

Lignin is a widely available, low-cost biobased polymer that shows promise as a component for SLS. In this work, PA12 powder was partially replaced by alkali lignin to demonstrate the possibility of reducing costs while maintaining the thermomechanical performance and, possibly, endowing the system with new properties, given the contribution of the polyaromatic molecule. The dispersion of lignin improved the performance of the SLS composite and also enhanced the thermal stability and the wettability of the structure. Our SLS structures, produced

with different orientations (horizontally flipped by 90°, flat, and vertically) were compared for their mechanical and other properties. The processing orientation was important in achieving a higher mechanical strength since higher number of horizontal layers result in improved strength up to two times higher compared to the sample processed in a flat orientation.

ASSOCIATED CONTENT

Supporting information includes: **Figure S1.** The selective fusion of unscanned areas in the selective laser sintering process of lignin/PA samples. **Figure S2.** The DTG of pure lignin. **Figure S3.** DSC scans of lignin/PA mixed in 60:40 vol% ratio before sintering and obtained during heating and cooling cycles (from 0 °C to 220 °C). **Figure S4.** for the thermogravimetric analysis of lignin/PA mixed at a 60:40 vol% ratio before sintering, from room temperature to 600 °C. **Figure S5.** Isothermal linear plot of adsorption and desorption for samples sintered at (a) 90°, and (b) flat orientation. **Table S1.** The latent heat of melting (ΔH_m), melting temperature (T_m), crystalline temperature (T_c) of mixed lignin and PA powder before sintering.

AUTHOR INFORMATION

Corresponding Author: orlando.rojas@aalto.fi, [+358505124227](tel:+358505124227)

Rubina Ajdary: <https://orcid.org/0000-0003-1193-8662>

Niklas Kretschmar: <https://orcid.org/0000-0002-0172-9528>

Hossein Baniyadi: <https://orcid.org/0000-0002-0463-337X>

John Trifol: <https://orcid.org/0000-0001-9447-1089>

Jukka V. Seppälä: <https://orcid.org/0000-0001-7943-3121>

Jouni Partanen: <https://orcid.org/0000-0002-4708-4833>

Orlando J. Rojas: <https://orcid.org/0000-0003-4036-4020>

Author Contributions

The manuscript was written through the contributions of all authors. All authors have approved the final version of the manuscript.

ACKNOWLEDGMENTS

RA and NK contributed equally to this work. We acknowledge funding support by the Academy of Finland's Biofuture 2025 program under project 2228357-4 (3D Manufacturing of Novel Biomaterials). RA acknowledges funding from the Finnish Foundation for Technology Promotion (TES). We acknowledge the help from Tuomas Puttonen for the design of the lattice structures. This work made use of the facilities of Aalto University's Nanomicroscopy Center and Aalto's ADDLAB.

References

- (1) Zhao, C.; Huang, J.; Yang, L.; Yue, F.; Lu, F. Revealing Structural Differences between Alkaline and Kraft Lignins by HSQC NMR. *Ind. Eng. Chem. Res.* **2019**, *58* (14), 5707–5714. <https://doi.org/10.1021/acs.iecr.9b00499>.
- (2) Li, J.; Zhang, J.; Zhang, S.; Gao, Q.; Li, J.; Zhang, W. Alkali Lignin Depolymerization under Eco-Friendly and Cost-Effective NaOH/Urea Aqueous Solution for Fast Curing Bio-Based Phenolic Resin. *Ind. Crops Prod.* **2018**, *120* (April), 25–33. <https://doi.org/10.1016/j.indcrop.2018.04.027>.
- (3) Fache, M.; Boutevin, B.; Caillol, S. Vanillin Production from Lignin and Its Use as a Renewable Chemical. *ACS Sustain. Chem. Eng.* **2016**, *4* (1), 35–46. <https://doi.org/10.1021/acssuschemeng.5b01344>.
- (4) Khan, T. A.; Lee, J. H.; Kim, H. J. *Lignin-Based Adhesives and Coatings*; 2019.

<https://doi.org/10.1016/B978-0-12-816354-2.00009-8>.

- (5) Rajesh Banu, J.; Kavitha, S.; Yukesh Kannah, R.; Poornima Devi, T.; Gunasekaran, M.; Kim, S. H.; Kumar, G. A Review on Biopolymer Production via Lignin Valorization. *Bioresour. Technol.* **2019**, *290* (July), 121790. <https://doi.org/10.1016/j.biortech.2019.121790>.
- (6) Liu, Q.; Luo, L.; Zheng, L. Lignins: Biosynthesis and Biological Functions in Plants. *Int. J. Mol. Sci.* **2018**, *19* (2). <https://doi.org/10.3390/ijms19020335>.
- (7) Chanoca, A.; de Vries, L.; Boerjan, W. Lignin Engineering in Forest Trees. *Front. Plant Sci.* **2019**, *10* (July). <https://doi.org/10.3389/fpls.2019.00912>.
- (8) Tarasov, D.; Leitch, M.; Fatehi, P. Lignin-Carbohydrate Complexes: Properties, Applications, Analyses, and Methods of Extraction: A Review. *Biotechnol. Biofuels* **2018**, *11* (1), 1–28. <https://doi.org/10.1186/s13068-018-1262-1>.
- (9) Gordobil, O.; Delucis, R.; Egüés, I.; Labidi, J. Kraft Lignin as Filler in PLA to Improve Ductility and Thermal Properties. *Ind. Crops Prod.* **2015**, *72*, 46–53. <https://doi.org/10.1016/j.indcrop.2015.01.055>.
- (10) Dai, L.; Cao, Q.; Wang, K.; Han, S.; Si, C.; Liu, D.; Liu, Y. High Efficient Recovery of L-Lactide with Lignin-Based Filler by Thermal Degradation. *Ind. Crops Prod.* **2020**, *143* (April 2019), 111954. <https://doi.org/10.1016/j.indcrop.2019.111954>.
- (11) Kohjiya, S.; Kato, A.; Ikeda, Y. Rubber Reinforcement with Lignin. In *Reinforcement of Rubber*; Springer: Singapore, 2020. https://doi.org/https://doi.org/10.1007/978-981-15-3789-9_7.
- (12) Frigerio, P.; Zoia, L.; Orlandi, M.; Hanel, T.; Castellani, L. Application of Sulphur-Free Lignins as a Filler for Elastomers: Effect of Hexamethylenetetramine Treatment.

- BioResources* **2014**, 9 (1), 1387–1400. <https://doi.org/10.15376/biores.9.1.1387-1400>.
- (13) Mohamad Aini, N. A.; Othman, N.; Hussin, M. H.; Sahakaro, K.; Hayeemasae, N. Lignin as Alternative Reinforcing Filler in the Rubber Industry: A Review. *Front. Mater.* **2020**, 6 (January). <https://doi.org/10.3389/fmats.2019.00329>.
- (14) Gao, Y.; Qu, W.; Liu, Y.; Hu, H.; Cochran, E.; Bai, X. Agricultural Residue-Derived Lignin as the Filler of Polylactic Acid Composites and the Effect of Lignin Purity on the Composite Performance. *J. Appl. Polym. Sci.* **2019**, 136 (35), 1–9. <https://doi.org/10.1002/app.47915>.
- (15) Yang, J.; Ching, Y. C.; Chuah, C. H. Applications of Lignocellulosic Fibers and Lignin in Review, Bioplastics A. *Polymers (Basel)*. **2019**, 11 (751).
- (16) Meyers, R. A. *Encyclopedia of Sustainability Science and Technology Series, Green Chemistry and Chemical Engineering*; 1997; Vol. 52. [https://doi.org/10.1016/s0009-2509\(97\)00005-5](https://doi.org/10.1016/s0009-2509(97)00005-5).
- (17) Kai, D.; Tan, M. J.; Chee, P. L.; Chua, Y. K.; Yap, Y. L.; Loh, X. J. Towards Lignin-Based Functional Materials in a Sustainable World. *Green Chem.* **2016**, 18 (5), 1175–1200. <https://doi.org/10.1039/c5gc02616d>.
- (18) Xu, W.; Wang, X.; Sandler, N.; Xu, C. Three-Dimensional Printing of Wood-Derived Biopolymers: A Review Focused on Biomedical Applications. *ACS Sustain. Chem. Eng.* **2018**, 6, 5663–5680. <https://doi.org/10.1021/acssuschemeng.7b03924>.
- (19) Sutton, J. T.; Rajan, K.; Harper, D. P.; Chmely, S. C. Lignin-Containing Photoactive Resins for 3D Printing by Stereolithography. *ACS Appl. Mater. Interfaces* **2018**, 10 (42), 36456–36463. <https://doi.org/10.1021/acsami.8b13031>.
- (20) ARBOFORM bioplastics <https://bioplastics.com.au/our-raw-materials/arboform/>.

- (21) Kumar, S. Selective Laser Sintering: A Qualitative and Objective Approach. *Jom* **2003**, 55 (10), 43–47. <https://doi.org/10.1007/s11837-003-0175-y>.
- (22) Schmid, M.; Amado, A.; Wegener, K. Polymer Powders for Selective Laser Sintering (SLS). *AIP Conf. Proc.* **2015**, 1664 (May). <https://doi.org/10.1063/1.4918516>.
- (23) Bakshi, K. R. A Review on Selective Laser Sintering: A Rapid Prototyping Technology. *IOSR J. Mech. Civ. Eng.* **2016**, 04 (04), 53–57. <https://doi.org/10.9790/1684-15008040453-57>.
- (24) Drummer, D.; Harder, R.; Witt, G.; Wegner, A.; Wudy, K.; Drexler, M. Long-Term Properties of Laser Sintered Parts of Polyamide 12. *Int. J. Recent Contrib. from Eng. Sci. IT* **2015**, 3 (1), 20–27.
- (25) Wudy, K.; Drummer, D. Aging Effects of Polyamide 12 in Selective Laser Sintering: Molecular Weight Distribution and Thermal Properties. *Addit. Manuf.* **2019**, 25 (November 2018), 1–9. <https://doi.org/10.1016/j.addma.2018.11.007>.
- (26) Hong, R.; Zhao, Z.; Leng, J.; Wu, J.; Zhang, J. Two-Step Approach Based on Selective Laser Sintering for High Performance Carbon Black/ Polyamide 12 Composite with 3D Segregated Conductive Network. *Compos. Part B Eng.* **2019**, 176 (June), 107214. <https://doi.org/10.1016/j.compositesb.2019.107214>.
- (27) BASF. *Technical Data Sheet for Ultrasint PA11*; 2019.
- (28) Shahini, A.; Yazdimamaghani, M.; Walker, K. J.; Eastman, M. A.; Hatami-Marbini, H.; Smith, B. J.; Ricci, J. L.; Madihally, S. V.; Vashae, D.; Tayebi, L. 3D Conductive Nanocomposite Scaffold for Bone Tissue Engineering. *Int. J. Nanomedicine* **2013**, 9 (1), 167–181. <https://doi.org/10.2147/IJN.S54668>.
- (29) Kun, D.; Pukánszky, B. *Polymer/Lignin Blends: Interactions, Properties, Applications*;

- 2017; Vol. 93. <https://doi.org/10.1016/j.eurpolymj.2017.04.035>.
- (30) Tejado, A.; Peña, C.; Labidi, J.; Echeverria, J. M.; Mondragon, I. Physico-Chemical Characterization of Lignins from Different Sources for Use in Phenol-Formaldehyde Resin Synthesis. *Bioresour. Technol.* **2007**, *98* (8), 1655–1663. <https://doi.org/10.1016/j.biortech.2006.05.042>.
- (31) Salmoria, G. V.; Leite, J. L.; Vieira, L. F.; Pires, A. T. N.; Roesler, C. R. M. Mechanical Properties of PA6/PA12 Blend Specimens Prepared by Selective Laser Sintering. *Polym. Test.* **2012**, *31* (3), 411–416. <https://doi.org/10.1016/j.polymertesting.2011.12.006>.
- (32) Zhao, M.; Wudy, K.; Drummer, D. Crystallization Kinetics of Polyamide 12 during Selective Laser Sintering. *Polymers (Basel)*. **2018**, *10* (2). <https://doi.org/10.3390/polym10020168>.
- (33) De Oliveira Setti, G.; De Silva, J. V. L.; De Oliveira, M. F.; Maia, I. A.; De Jesus, D. P.; Savu, R.; De Almeida Santos, T. E.; De Cássia Zacardi De Souza, R.; Joanni, E. Surface Methods for Monitoring the Densification of Parts in the Selective Laser Sintering Process. *Rapid Prototyp. J.* **2014**, *20* (2), 157–163. <https://doi.org/10.1108/RPJ-05-2012-0040>.
- (34) Yap, C. Y.; Chua, C. K.; Dong, Z. L.; Liu, Z. H.; Zhang, D. Q.; Loh, L. E.; Sing, S. L. Review of Selective Laser Melting: Materials and Applications. *Appl. Phys. Rev.* **2015**, *2* (4). <https://doi.org/10.1063/1.4935926>.
- (35) Pilipović, A.; Brajliah, T.; Drstvenšek, I. Influence of Processing Parameters on Tensile Properties of SLS Polymer Product. *Polymers (Basel)*. **2018**, *10* (11). <https://doi.org/10.3390/polym10111208>.

- (36) Rahim, T. N. A. T.; Abdullah, A. M.; Akil, H. M.; Mohamad, D. Comparison of Mechanical Properties for Polyamide 12 Composite-Based Biomaterials Fabricated by Fused Filament Fabrication and Injection Molding. *AIP Conf. Proc.* **2016**, *1791*. <https://doi.org/10.1063/1.4968862>.
- (37) Ma, N.; Liu, W.; Ma, L.; He, S.; Liu, H.; Zhang, Z.; Sun, A.; Huang, M.; Zhu, C. Crystal Transition and Thermal Behavior of Nylon 12. *e-Polymers* **2020**, *20* (1), 346–352. <https://doi.org/10.1515/epoly-2020-0039>.
- (38) Roy, S.; Das, T.; Zhang, L.; Li, Y.; Ming, Y.; Ting, S.; Hu, X.; Yue, C. Y. Triggering Compatibility and Dispersion by Selective Plasma Functionalized Carbon Nanotubes to Fabricate Tough and Enhanced Nylon 12 Composites. *Polymer (Guildf)*. **2015**, *58* (December 2018), 153–161. <https://doi.org/10.1016/j.polymer.2014.12.032>.
- (39) Zhou, C.; Qi, S.; Zhu, P.; Zhao, Y.; Xu, Y.; Dong, X.; Wang, D. The Methylene Infrared Vibration and Dielectric Behavior Monitored by Amide Group Arrangement for Long Chain Polyamides. *Polymer (Guildf)*. **2020**, *190* (November 2019), 122231. <https://doi.org/10.1016/j.polymer.2020.122231>.
- (40) Lu, Y.; Lu, Y. C.; Hu, H. Q.; Xie, F. J.; Wei, X. Y.; Fan, X. Structural Characterization of Lignin and Its Degradation Products with Spectroscopic Methods. *J. Spectrosc.* **2017**, *2017*. <https://doi.org/10.1155/2017/8951658>.
- (41) Ma, Z.; Sun, Q.; Ye, J.; Yao, Q.; Zhao, C. Study on the Thermal Degradation Behaviors and Kinetics of Alkali Lignin for Production of Phenolic-Rich Bio-Oil Using TGA-FTIR and Py-GC/MS. *J. Anal. Appl. Pyrolysis* **2016**, *117*, 116–124. <https://doi.org/10.1016/j.jaap.2015.12.007>.
- (42) Deng, Z.; Xia, A.; Liao, Q.; Zhu, X.; Huang, Y.; Fu, Q. Laccase Pretreatment of Wheat Straw: Effects of the Physicochemical Characteristics and the Kinetics of Enzymatic

- Hydrolysis. *Biotechnol. Biofuels* **2019**, *12* (1). <https://doi.org/10.1186/s13068-019-1499-3>.
- (43) Abbati De Assis, C.; Greca, L. G.; Ago, M.; Balakshin, M. Y.; Jameel, H.; Gonzalez, R.; Rojas, O. J. Techno-Economic Assessment, Scalability, and Applications of Aerosol Lignin Micro- and Nanoparticles. *ACS Sustain. Chem. Eng.* **2018**, *6* (9), 11853–11868. <https://doi.org/10.1021/acssuschemeng.8b02151>.
- (44) Lourencon, T. V.; Greca, L. G.; Tarasov, D.; Borrega, M.; Tamminen, T.; Rojas, O. J.; Balakshin, M. Y. Lignin-First Integrated Hydrothermal Treatment (HTT) and Synthesis of Low-Cost Biorefinery Particles. *ACS Sustain. Chem. Eng.* **2020**, *8* (2), 1230–1239. <https://doi.org/10.1021/acssuschemeng.9b06511>.
- (45) Varotsis, A. B. Introduction to SLS 3D printing <https://www.3dhubs.com/knowledge-base/introduction-sls-3d-printing/>.
- (46) Liu, L.; Lin, M.; Xu, Z.; Lin, M. Polylactic Acid-Based Wood-Plastic 3D Printing Composite and Its Properties. *BioResources* **2019**, *14* (4), 8484–8498. <https://doi.org/10.15376/biores.14.4.8484-8498>.
- (47) Tanase-Opedal, M.; Espinosa, E.; Rodríguez, A.; Chinga-Carrasco, G. Lignin: A Biopolymer from Forestry Biomass for Biocomposites and 3D Printing. *Materials (Basel)*. **2019**, *12* (18), 1–15. <https://doi.org/10.3390/ma12183006>.
- (48) Li, J.; Chua, C. S. Transductive Inference for Color-Based Particle Filter Tracking. *IEEE Int. Conf. Image Process.* **2003**, *3* (July 2002), 949–952. <https://doi.org/10.1002/pi.1137>.
- (49) Zhang, S.; Li, M.; Hao, N.; Ragauskas, A. J. Stereolithography 3D Printing of Lignin-Reinforced Composites with Enhanced Mechanical Properties. *ACS Omega* **2019**, *4*

(23), 20197–20204. <https://doi.org/10.1021/acsomega.9b02455>.

- (50) Ibrahim, F.; Mohan, D.; Sajab, M. S.; Bakarudin, S. B.; Kaco, H. Evaluation of the Compatibility of Organosolv Lignin-Graphene Nanoplatelets with Photo-Curable Polyurethane in Stereolithography 3D Printing. *Polymers (Basel)*. **2019**, *11* (10). <https://doi.org/10.3390/polym11101544>.

For Table of Contents Use Only

Selective laser sintering of complex lignin-based structures as a development step toward lignin valorization in composites.

